XXXVI Ibero-Latin American Congress on Computational Methods in Engineering
CILAMCE
Rio de Janeiro, 22-25 Nov 2015

# AN UNBONDED FLEXIBLE PIPE FINITE ELEMENT MODEL

**Gonzalez, Gabriel Mattos**

**De Sousa, José Renato Mendes**

**Sagrilo, Luis Volnei Sudati**

gmattosg@gmail.com

jrenato@laceo.coppe.ufrj.br

sagrilo@coc.ufrj.br

LACEO – Programa de Engenharia Civil - COPPE/UFRJ - BRAZIL

Avenida Pedro Calmon s/nº, Cidade Universitária, 21941-972, Rio de Janeiro, RJ, Brazil

***Abstract.*** *Unbonded flexible pipes are multi-layered structures with their typical cross-section composed by a combination of steel armoring layers (inner carcass, tensile and pressure armors) and polymeric conduits and tapes. This paper presents a finite element model, entirely developed in ABAQUS® environment, fully capable of calculating stresses and strains in those several layers when subjected to different types of loads. The finite element model employs four nodes reduced integration shell elements. The inner layers, located bellow the first tensile armor, are condensed into a unique cylinder with its distinct properties well assured. The same assumption is applied to the layers placed above the second tensile armor. Moreover, rebar elements were considered for the carcass and pressure armor modeling. As for the tensile armors, each steel tendon is modeled individually by shell elements. The interactions between tensile armors tendons and between the tensile armors and the adjacent layers are handled with tangential and normal contact formulations. As a case study, a 2.5" unbonded flexible pipe is considered under pure tension. The results obtained are compared to an existing analytical model as well as from previously published experimental data. All results agreed quite well.*

***Keywords:*** *Finite Element Method, Structural Analysis, Unbonded Flexible Pipe.*

# 1 INTRODUCTION

Flexible risers are extensively used in floating production systems providing fluid and gas transport between the oil rig and seabed. These pipes may present a more feasible solution than conventional rigid risers because they do not require neither heave compensation and tensioning devices at the platform level nor riser manifolds at sea-bed. They also present higher resistance to fatigue and corrosion, and ease transportation, installation and storage.

The concept inherent to these pipes comprehends a combination of high compliance and capacity of deformation in bending, with high strength and stiffness in axisymmetric response. This contrasting behavior is achieved by combining polymeric conduits and helically settled steel tendons. While the first components are mainly responsible for sealing the pipe the latter are used to guarantee its structural integrity.

These armor layers are generally of three types: the interlocked steel carcass that prevents the collapse of the inner polymeric conduit due to external pressure; the pressure armor, a wound steel helix that provides radial resistance to external and internal pressure; and the tensile armors, a double cross-wound armoring layer which provides resistance to axial tension and torque. An example of a typical unbonded flexible riser cross-section is shown in Figure 1.

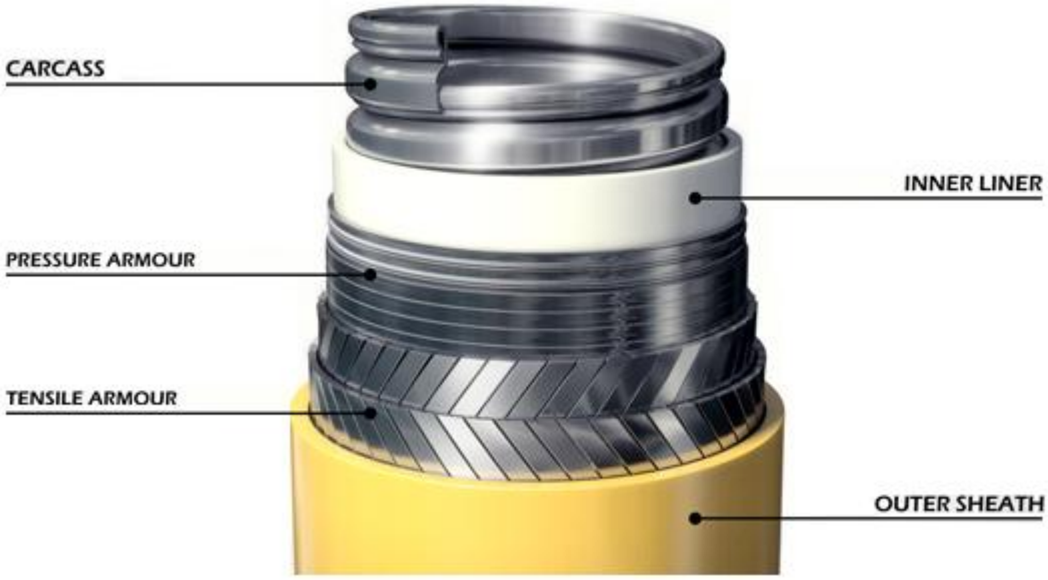


**Figure 1 – Unbonded flexible riser (NOV, 2015).**

Many authors have dedicated their efforts on the prediction of the structural behavior of such composite structures. Next, the main developments in this area are briefly described, focusing on the studies which emphasize the axisymmetric response of these pipes.

Knapp (1979) derived a stiffness matrix for straight composite cable element considering its axisymmetric response. The author addressed the axisymmetric response of an aluminum core with steel helical reinforcement cables. Despite the nonlinearity considered for deriving the formulation, a linear elastic matrix is presented and compared to experimental results presenting good correlation.

Considering the flexible pipes as a perfectly gathering of concentric tubular and helical armor layers, Feret et al. (1986) formulated a set of linear equations that govern their axisymmetric response. These equations became one of the first analytical models suited for describing the axisymmetric response of flexible pipes.

Batista et al. (1989) systematized a slightly different set of linear equations also capable of predicting the axisymmetric behavior of flexible pipes. These authors considered the interactions between adjacent layers in bonded and unbonded situations. These equations are used for comparison purposes in this paper due to its simplicity and efficiency; therefore they shall be further described.

Witz and Tan (1991) developed a nonlinear analytical model for the axial-torsional behavior of flexible pipes under moderate loads. This model considers the polymeric layers as thin-walled cylinders and the armor tendons governed by Love's equilibrium equations of elastic helices without pre-twist. Authors presented three cases of study: a typical marine cable, a flexible riser and an umbilical cable. The results were compared to tensile tests and shown quite satisfactory agreement.

Saevik (1993) studied the stress and strain behavior of a single tensile armor tendon by proposing an eight degree of freedom curved beam finite element (FE) submitted to a given curvature distribution. The conception of such elements is linked to the assumption of a kinematical constraint that imposes their slide to occur only on the surface of a supporting pipe. An 8m long 5" diameter pipe was submitted to an experimental test and results were compared to the ones obtained by the numerical model considering constant and varying curvature. The numerical results were in very good agreement with the experimental ones. Although it was only studied the bending response of the tendon, the FE formulation should also permit the study of the pipe's axisymmetric behavior.

Witz (1996) carried an experimental study on a 2.5" flexible pipe in which he sought to evaluate the influence of the boundary conditions on the axial and torsional stiffness of the pipe. Several institutions were asked to reproduce Witz's results with their models. The comparisons showed good correlation concerning the axial stiffness, but not as good agreement was obtained for the torsional results.

Custódio and Vaz (2002) developed a nonlinear analytical model to represent the response of slender tubular structures, such as umbilical cables and flexible risers. The homogeneous and helical armor layers are described respectively by Lame´'s and Clebsch–Kirchhoff's formulations. Material nonlinearities, gap formation and inter-wire contact were taken into account in this model. Finally, a flexible pipe and a marine umbilical cable were studied under moderate pulling and torque loads.

Sousa (2005) proposed, for local analysis, an unbonded flexible riser FE model based on beams, shells and normal contacts elements entirely developed in *ANSYS*®. It was carried a meticulously theoretical study on riser's local behavior, which was presented against experimental data.

Ramos et al. (2008) conducted a series of experimental tests on a 2.5" flexible pipe alternating axial tension with and without internal pressure. The influence of boundary conditions on its response was also analyzed. The results were compared to a previously proposed model (Ramos and Pesce, 2004), which was able to well predict the axial stiffness as well as the strains in the outer armor tendons.

Bathui (2008a) and (2008b) investigated the response of a five-layer flexible pipe under pure tension (2008a) and torsion (2008b) by means of a detailed nonlinear solid threedimensional FE model, which uses the Coulomb frictional model for representing the interactions between the riser's layers. The model was capable of well reproducing these interactions as well as pipe's overall structural response. However, as the model is constituted by solid components and all the interactions are accounted for, it turned out to be a very computer demanding numerical model.

Merino et al. (2009) and (2010) studied the response of a 4" flexible pipe when submitted to pure axial tension (2009), to pure torsion and torsion combined with axial tension (2010). All tests results obtained were compared to the prediction performed by Sousa's (2005) nonlinear FE model and presented good agreement for all cases studied. Two remarks were of great importance: the friction was noticed as a key aspect for correctly predicting torsional response; and the resulting twist showed a nonlinear variation with the imposed tension load in the pure tension case.

Recently, Saevik (2011) has proposed three different models for predicting stresses in tensile armor layers of unbonded flexible pipes. While one model is focused on the axisymmetric response of the armor tendons, the others two are responsible for predicting their bending stresses. All the formulations were based on large displacements and small strains theory. The models were further validated using experimental data of an 8" flexible riser.

In this work it is proposed a numerical model based on FE method and entirely developed in *ABAQUS®*. The finite element model is mainly described by shell elements. It is fully capable of calculating all layers' stresses and strains, although the focus is giving on the response of the tensile armor layers. A parametric study concerning contact definition is performed through the FE model of a 2.5" unbonded flexible pipe under pure tension. Both Batista et al.'s (1989) analytical model and previously published experimental data are used for comparison matters.

Next, Batista et al. (1989) analytical model will be briefly described followed by the description of the FE model proposed in this work, of the case of study, of the results obtained and, finally, the conclusions found in this research are described.

## 2 ANALYITCAL MODEL

The analytical model presented in this section was developed by Batista et al. (1989) for local structural analysis of both bonded and unbonded flexible risers when subjected to axisymmetric loads. It was developed based on six simplifying hypotheses, as described below:

i. the pipe works within the small strain domain;

ii. all layers are subjected to the same axial strain and rotation;

iii. the pipe cross sections remain plane after deformation;

iv. all materials are stressed within the range of the linear elastic theory;

v. there is no loss of contact between the layers; and

vi. the linear superposition of effects is valid.

This formulation allows the representation of an arbitrary numbers of layers ($N$+$M$), where $M$ represents the number of elastomeric layers and $N$ the number of metallic armors. It leads to a linear system of equations with 6$N$+6$M$+2 unknowns, which are:

| | |
|---|---|
| axial, radial and shear strains | ($N$+$M$+2); |
| external final radius | (1); |
| contact pressure between layers | ($N$+$M$-1); |
| thickness variation | ($N$+$M$); |
| laying angles | ($N$); |
| tension in the armors | (2$N$); |
| and tension in the elastomeric layers | (3$M$). |

It is not necessary, however, to perform the calculation of all these unknowns, once only $N$+$M$+2 are considered not redundant. Hence, only the main unknowns – i.e. axial, radial and shear strains – are utilized in order to solve the resulting linear system of equations. The others 5$N$+5$M$ unknowns are obtained by relations involving the main variables.

The model is composed of two distinct kinds of equations, which combined will generate the previously mentioned linear equations system. The first sort of equations consists of three equilibrium equations, i.e., the equilibrium between axial forces, torsion moments and radial pressures. The second is named compatibility equations. These equations should ensure that no gaps between layers are observed. The equilibrium equations are presented in the following form:

$$R_{s,*}(\sigma_{t_j}, \alpha_j) + R_{m,*}(\sigma_L, \sigma_\theta) + R_{b,*}(Pc_j, \tau_j) = F_* \tag{1}$$

Equation (1) states that the sum of the force contributions from the different components or layers of the pipe as well as their interactions is equal to the applied external force. The difference inherent to each layer will reveal itself as a distinct mechanical contribution; consequently two different sets of equation shall be presented: one for representing the armor (Table 1) and one for representing the elastomeric layers (Table 2). Table 3 shows the contribution regarding to the interaction between two adjacent layers and Table 4 shows the applied external forces.

**Table 1 – Contribution of armor components.**

| $\mathbf{R_{s,z}}$ | $\mathbf{R_{s,\varphi}}$ | $\mathbf{R_{s,r}}$ |
|---|---|---|
| $\sum_{j=1}^{N} n_j \sigma_{t_j} A_j \cos(\alpha_j)$ | $\sum_{j=1}^{N} n_j \sigma_{t_j} A_j a_j \sin(\alpha_j) + n_j J_j G_j \cos^2(\alpha_j)\, \delta\emptyset$ | $\dfrac{n_j \sigma_{t_j} A_j \cos(\alpha_j)}{L_j}$ |

**Table 2 – Contribution of elastomeric layers.**

| $R_{m,z}$ | $R_{m,\varphi}$ | $R_{m,r}$ |
|---|---|---|
| $\sum_{j=1}^{M} \sigma_{L_j} A_{m_j}$ | $\sum_{j=1}^{M} G_{m_j} J_{m_j} V_{m_j} \delta\emptyset$ | $\frac{1}{2}\sigma_{\theta_j} e_j$ |

**Table 3 – Contribution of the shear stress originated by the interaction between armor and elastomeric layers.**

| $R_{b,z}$ | $R_{b,\varphi}$ | $R_{b,r}$ |
|---|---|---|
| $\sum_{j=1}^{N} n_j P_{c_j} (\frac{a_j - e_j}{2})\, b_j \tan(\alpha_j)$ | $\sum_{j=1}^{N} n_j \mu_j P_{c_j} (\frac{a_j - e_j}{2})\,(2\pi a_j l_j)/b_j$ | $n_j \mu_j P_{c_j} (\frac{a_j - e_j}{2})\,(2\pi a_j l_j)/b_j$ |

**Table 4 – External resultant applied forces.**

| $F_z$ | $F_\varphi$ | $F_r$ |
|---|---|---|
| $F + \beta\pi(P_{int} a_{int}{}^2 - P_{ext} a_{ext}{}^2)$ | $T$ | $P_{c_j}(a_j - e_j/2) - P_{c_{j+1}}(a_{j+1} - e_{j+1}/2)$ |

Finally, the stress-strain behavior is described as function of the main unknowns. Therefore, for the elastomeric layers both axial and circumferential stresses are given in Table 5, whereas the response of the armor components, both axial and shear stresses, are given in Table 6.

**Table 5- Axial and circumferential stress due to elastomeric layers response.**

| Elastomeric stress | |
|---|---|
| Axial | $\sigma_{L_j} = \frac{E_j}{(1 - \nu_j^2)}[\varepsilon_z + \varepsilon_y \nu_j]$ |
| Circumferential | $\sigma_{\theta_j} = \frac{E_j}{(1 - \nu_j^2)}[\varepsilon_y + \varepsilon_z \nu_j]$ |

**Table 6 - Axial and shear stress due to armor tendons response.**

| Armor stress | |
|---|---|
| Axial | $\sigma_{t_j} = E[\varepsilon_z \cos^2(\alpha_j) + \varepsilon_y \sin^2(\alpha_j) + a.\,\delta\emptyset.\sin(\alpha_j)\cos(\alpha_j)]$ |
| Shear | $\tau_{L_j} = G_m\left[(\varepsilon_z - \varepsilon_y)\sin(\alpha_j)\cos(\alpha_j) + \frac{1}{2}a.\,\delta\emptyset.\cos(2\alpha_j)\right]$ |

These, along with the radius compatibility equations, can be gathered in a linear system of equations, which, due to its non-singularity, can be easily solved by any linear equations system's solving method. In this work it was utilized a LU decomposition method.

# 3 FINITE ELEMENT MODEL

The FE model was developed in *ABAQUS®* (see Figure 2) and represents, three-dimensionally, the local structural behavior of multi-layered unbonded flexible pipes. In what follows, the FE techniques employed for the representation of each of pipe's layers is detailed as well as the interactions between them.

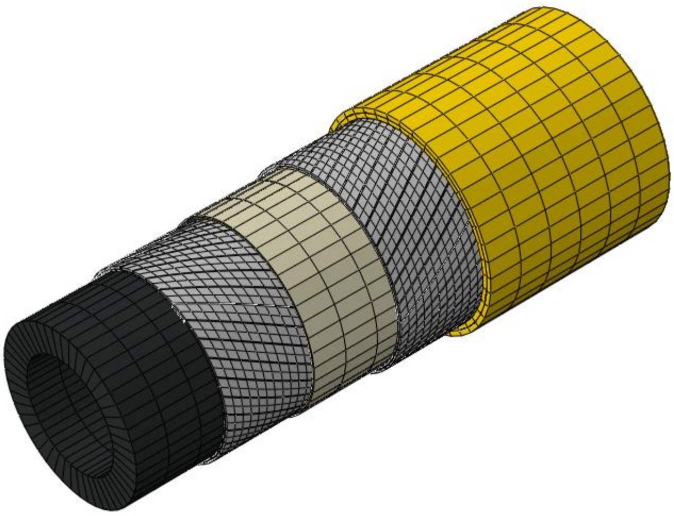

**Figure 2 - Finite element model proposed.**

The model consists, mainly, of shell elements. Only the inner carcass and the pressure armor need an additional approach for their representation: the reinforcement technique called rebar. For computational efficiency matters, all the layers under the first set of tensile armor tendons were condensed into a single but equivalent composite shell. The same approach was adopted for the outer layers, i.e. the concentric layers located above the last set of tensile armor tendons. Each tendon that comprises the two cross-wounded armors layers is represented individually by shell elements.

Before entering in a more detailed description of the model, the coordinate systems and the wire numeration are presented in Figure 3.

## 3.1 Polymeric sheaths and tapes

The polymeric sheaths and tapes are considered layers of the four nodes reduced integration composite shell elements. The composite shell elements are defined to ensure computational efficiency and each layer is modeled according to its correspondent thickness, material and relative radial position.

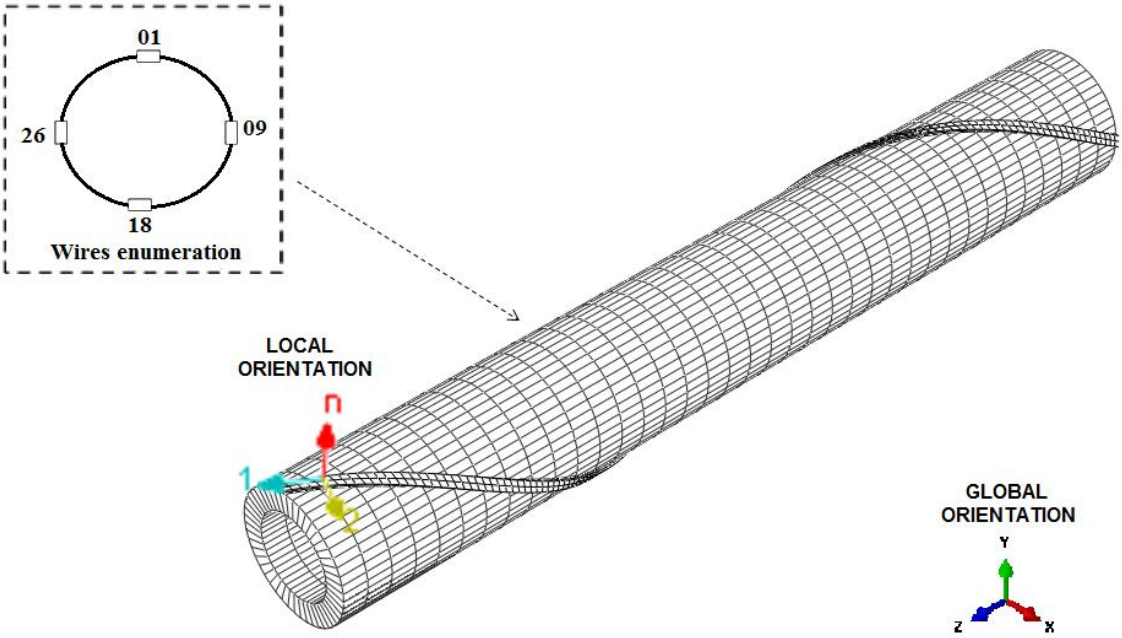


**Figure 3 – Wire numeration, local and global coordinates systems.**

## 3.2 Inner carcass and pressure armor

Both inner carcass and pressure armor are modeled as layers of the same composite shell elements, but additional wound reinforcement elements were also defined for these same layers. This approach was granted by a technique called REBAR elements. Those elements are defined by its cross-sectional area, the lay angle, the radial position of its inertial center and the space between two adjacent bars. To guarantee that this approach is equivalent to the mechanical behavior of metallic wound armors, it is important to adopt the distance between bars as one pitch, for the carcass, and half of the pitch, for the pressure armor (SIMULIA, 2013). Moreover, it is necessary to assume that some sort of material is evolving them. Still in order to guarantee the mechanical behavior, an auxiliary linear elastic material with very low Young modulus was used.

## 3.3 Tensile armor

The cross-wound tensile armors are also represented using four nodes reduced integration shell elements, where each tendon is modeled separately.

## 3.4 Contact between layers

The general contact algorithm, in *ABAQUS/Explicit*, was used for detection of contacting surfaces because of its efficiency, simplicity and capacity of edge to edge contact detection. Contact interactions between adjacent surfaces are defined considering both their normal and tangential properties. The normal behavior of contact is modeled with the Penalty method and, according to Sousa (2005), it is responsible for governing the pipe's axisymmetric response. Hence, model's axial behavior was studied with the variation of contact penalty stiffness, what will be shown further ahead in this work. As for the frictional behavior, the

Coulomb model was adopted, but only considering its stick representation (Bathui, 2008a). The friction coefficient varies between 0.03 and 0.07, according to Merino et al. (2009). Therefore, another parametric study was taken in order to determine the appropriate friction coefficient for the pure axial tension analysis.

# 4 CASE OF STUDY

## 4.1 Flexible riser's general properties

A 2.5" unbonded flexible riser was analyzed under pure tension. The pipe has a free span of 1.17m or two pitches of the outer tensile armor tendons. Physical and geometrical characteristics of the pipe are exposed in Table 7.

**Table 7 – Main characteristics of the 2.5" flexible pipe.**

| Layer (material) | Properties |
|---|---|
| Inner carcass (AISI 304) | Internal diameter = 63.5mm; thickness = 3.5mm; number of wires = 1; lay angle = +87.6°; cross-section area = 19.6mm²; moment of inertia = 23.1mm$^4$; Young modulus = 205GPa; Poisson ratio = 0.3 |
| Internal plastic (polyamide 11) | thickness = 5.0mm; Young modulus = 345MPa; Poisson ratio = 0.45 |
| Pressure armor (carbon steel) | thickness = 6.2mm; number of wires = 2; lay angle = +85.6°; cross-section area = 54.1mm²; moment of inertia = 173.4mm$^4$; Young modulus = 205GPa; Poisson ratio = 0.3 |
| Anti-wear tape (polyamide 11) | thickness = 2.0mm; Young modulus = 205GPa; Poisson ratio = 0.40 |
| Inner tensile armor (carbon steel) | thickness = 2.5mm; number of wires = 32; lay angle = +30.0°; cross-section area = 12.0mm²; moment of inertia = 10.42mm$^4$; Young modulus = 205GPa; Poisson ratio = 0.3 |
| Anti-wear tape (polyamide 11) | thickness = 1.5mm; Young modulus = 345MPa; Poisson ratio = 0.40 |
| Outer tensile armor (carbon steel) | thickness = 2.5mm; number of wires = 34; lay angle = -30.0°; cross-section area = 12.0mm²; moment of inertia = 10.42mm$^4$; Young modulus = 205GPa; Poisson ratio = 0.3 |
| Fabric Tape | thickness = 0.5mm; Young modulus = 345MPa; Poisson ratio = 0.40 |
| External plastic (polyamide 11) | thickness = 5.0mm; Young modulus = 215MPa; Poisson ratio = 0.45 |

## 4.2 Mesh properties, boundary conditions and application of the loads

A 1.17m long model was meshed layer by layer. The concentric layers hold the same number of divisions. All the armor's tendons were also equally meshed. However, a finer mesh was employed to these latest structural components. The model consist of 57810 nodes, 40984 shell elements and 11712 rebar elements leading to 245904 degrees of freedom. Figure 4 illustrates the mesh adopted.

The boundary conditions were applied at both ends of the model in order to permit the application of the different loads without facing any numerical singularity. This boundary conditions as well as the loads were imposed on reference points – located in the origin and in the end of model's central axis, see detail in Figure 4 –, which were rigidly coupled to all nodes from the first and last cross-sections by a rigid beam constraint called Multi-Points Constraint or MPC (DS Simulia, 2010). It is important to highlight that only the axial displacement of the end of the model is set free and all other degrees of freedoms are restrained.

Additionally, it is worth noticing that, as the dynamic explicit module of *ABAQUS®* is used, due to the several contacts surfaces that need to be solved, the pulling load was applied linearly and slowly along time evolution. This process guarantees the model not to be subjected to any dynamic response, in other words, guarantees a quasi-static analysis. The final magnitude of the load, 700.00 kN, was chosen because it is approximately to half of the estimated damaging pull of the flexible pipe (Sousa, 2005).

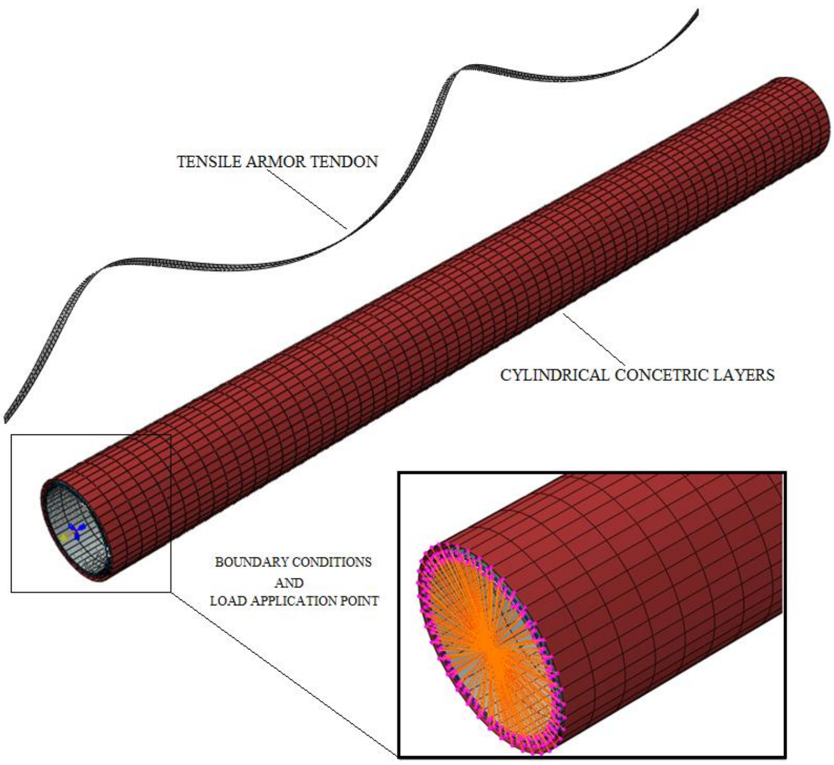


**Figure 4 – Mesh, load application point and boundary conditions.**

## 5 RESULTS AND DISCUSSIONS

This section aims to present the numerical and analytical results obtained in a pure tension analysis and compare them with previously published experimental data by Sousa et al (2013).

Before any further discussions on the stress/strain behavior of the flexible pipe, the FE model was submitted to a parametric study concerning its contact constants, the normal stiffness and the friction coefficient. The parametric variation analyzed can be seen in Table 8.

**Table 8 – Parametric study cases.**

| Case's label | Normal Stiffness (k)* | Friction Coefficient (μ)** |
|---|---|---|
| *nk_10* | 10.00 | |
| *nk_100* | 100.00 | |
| *nk_1000* | 1000.00 | 0.10 |
| *nk_10000* | 10000.00 | |
| *nk_100000* | 100000.00 | |
| *mu_003* | | 0.03 |
| *mu_005* | | 0.05 |
| *mu_007* | 5000.00 | 0.07 |
| *mu_010* | | 0.10 |
| *mu_013* | | 0.13 |

* [N/mm³]; ** Dimensionless

The first set of analysis considered the variation of normal contact stiffness and, as stated by Sousa (2005), a correct definition of this parameter is fundamental for a good correlation between FE model and experimental results, when it is subjected to pure tension. In Figure 5, the axial displacement evolution due to tension's increment is plotted for the several numerical cases proposed as well as for the analytical and the experimental results. It is important to notice that the pulling load increment in the graph was shown as dimensionless parameter.

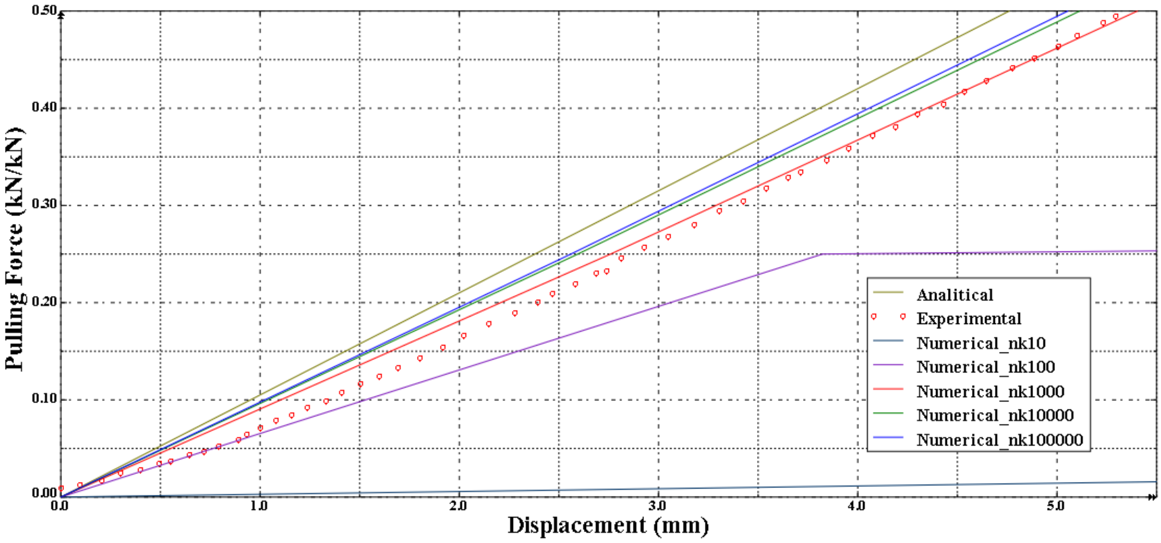


**Figure 5 – Displacement *vs.* Pulling load for normal contact stiffness variation.**

Figure 5 indicates that the *Numerical_nk10* and *Numerical_nk100* models do not represent well the response of the pipe. In the first case, the curve shows no physical correspondence with pipe's behavior whatsoever. The second case, though, suggests that lower normal contact stiffness might be used for small loads applications (smaller than 100kN), such as those used for obtaining pipe's axial stiffness or predicting small axial displacements, without a great lose in behavior correspondence. The main advantage in using lower normal contact parameter is the reduction of computational time spent for the numerical analysis.

The global axial stiffness of the flexible pipe was calculated and it is presented in Table 9. The results indicated that the increase in the normal contact stiffness will provide a greater value of axial global stiffness. This correspondence was already expected. The influence of normal contact stiffness in the global axial behavior of the model may be given by an asymptotic function which tends to 160 MN. Therefore, to well represent pipe's axial structural behavior, the optimal contact stiffness shall be comprehended in between 1000 N/mm³ and 10000 N/mm³.

**Table 9 – Axial stiffness comparison.**

| EA – Axial Stiffness (MN) | | | | | | |
|---|---|---|---|---|---|---|
| Analytical | Experimental | Numerical | | | | |
| | | nk_10 | nk_100 | nk_1000 | nk_10000 | nk_100000 |
| 165 | 153* | - | 128** | 149 | 158 | 159 |

* Value obtained only considering the linear portion of the data; ** Value obtained considering the first linear ascendant results.

In the next set of analysis, the normal contact stiffness was assumed to be constant, 5000 N/mm³, and the tangential contact parameter was varied, according to Table 8. Figure 6 illustrates the pipe's response to the same pulling load for the five friction coefficients situations. As can be noticed in Figure 6, friction coefficient plays no important role when it comes to pipe's displacement response and, consequently, to its axial stiffness.

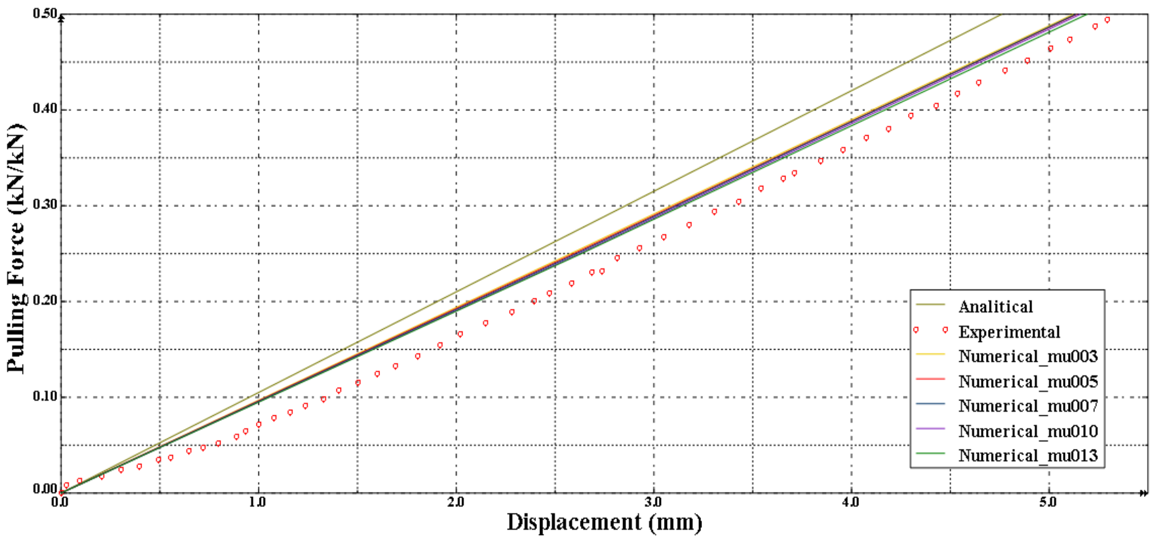


**Figure 6– Displacement vs. Pulling load for frictional coefficient variation.**

It was observed in the FE model, as well as stated by Sousa (2013) in the experimental tests after the accommodation phase, a linear variation in wire's stress/strain response along the increment of the load. Only the outer layer tendons were investigated in the experimental test. Therefore, Figure 7 illustrates the stresses obtained through the numerical and analytical model for half of the load analyzed (700kN). The experimental data is also shown in Figure 7.

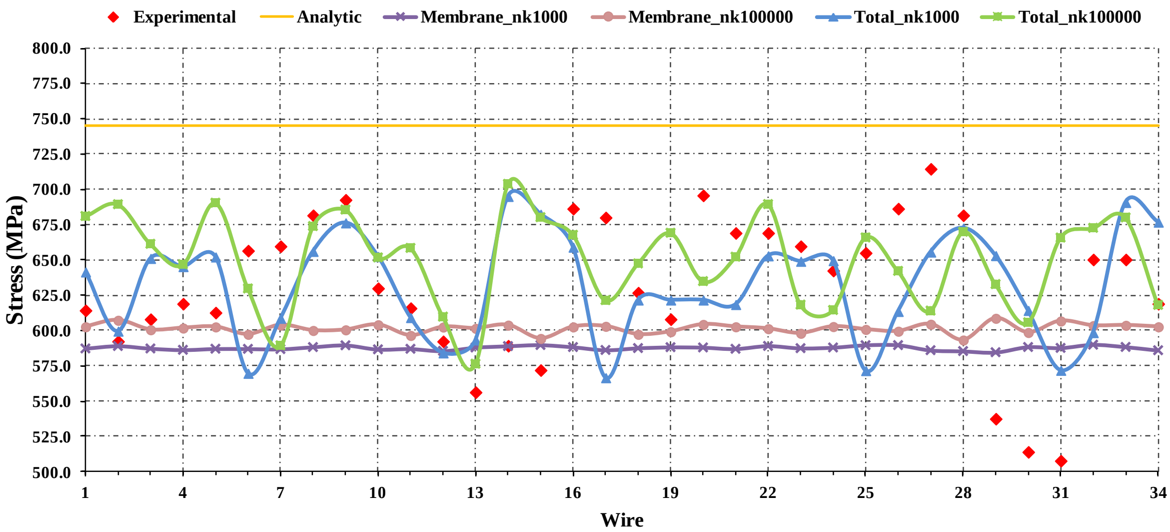


**Figure 7 – Comparison between analytical, experimental and numerical stress (MPa) on wires.**

Figure 7 shows both total and membrane stresses for two chosen numerical cases (*nk_1000* and *nk_100000*) in order to facilitate the visualization of the results. However, for the remaining cases, Table 10 gives tendons total and membrane stresses by means of their average and standard deviation for a section in the middle of the model.

One should observe from Figure 7 that, despite the differences in individually tendons' results, the FE model is capable of calculating a pretty assertive average and a quite satisfactory standard deviation, if one considers that an experimental test carries some inherent uncertainties.

**Table 10 – Tendon's stress comparison.**

| Case's label | Wire's stress | | | |
|---|---|---|---|---|
| | Membrane | | Total | |
| | average* | standard deviation** | average* | standard deviation** |
| *Analytical* | - | - | 745.00 | - |
| *Experimental* | - | - | 630.83 | 51.92 |
| *Sousa (2005)* | 595.35 | - | - | - |
| *nk_1000* | 587.62 | 1.36 | 631.89 | 37.98 |
| *nk_10000* | 599.91 | 2.13 | 646.87 | 33.12 |
| *nk_100000* | 601.57 | 3.45 | 650.36 | 31.92 |
| *mu_003* | 598.60 | 3.41 | 653.09 | 31.88 |
| *mu_005* | 593.53 | 3.01 | 639.47 | 33.72 |
| *mu_007* | 598.16 | 2.65 | 645.81 | 35.55 |
| *mu_010* | 597.95 | 2.44 | 646.94 | 31.26 |
| *mu_013* | 595.75 | 2.94 | 644.93 | 27.38 |

* [MPa]; ** [MPa]

Analyzing Table 10, one can observe that the influence of contact parameters on the calculation of tendons' stresses does not present a very clear and definitive correlation for all cases. This is attributed to the nonlinearities imposed by the contact formulations and the explicit algorithm used to solve the differential equations.

In spite of the lack of correlation mentioned above, some inferences can be made, such as: an increase in normal contact stiffness will also provide an increase, though not proportional, in both stresses' averages and in membrane's standard deviation. The opposite is noted on total stress's standard deviation behavior, which decreases for greater normal contact stiffness.

Another remark concerns the tangential contact parameter variation. The membrane stress's averages were almost kept constant for all cases – less than 1% of deviation from the larger (*mu_003*) to the smaller (*mu_005*) was found. The remaining results, on the other hand, did not present any relevant relation that should be highlighted.

The results concerning the total axial stress averages were presented in quite good agreement with experimental results (varying from 0.17% to 3.53%), even noticing a fluctuation on the average and standard deviation due to the change on the contact parameter. Comparisons between numerical and experimental standard deviations were also promising. The deviation of the analytical result, when compared to the experimental average, was equal to 18.10%. This deviation shall be analyzed carefully, once it falls significantly (4.35%) when the maximum stress obtained in the test is chosen as reference.

The membrane stresses obtained were almost linear agreeing with Sousa's (2005) numerical model. The results obtained were equivalent to the previously mentioned model. Thus the average's deviations when compared Sousa's results to the results presented on this work were quite small (varying from 0.06% to 1.3%).

Finally, one can see the influence of bending stress in the tensile armoring tendons when the pipe is subjected to pure tension. As believed, the model predicted the bending stress of the tendons varying from 7.53% to 9.11% of the membrane stress. This shows the influence of local bending effect on tendons which some numerical models are not able to predict and gives a brief explanation on why experimental analysis presents no constant strain behavior on different tendons, as considered by many authors.

## CONCLUSION

In this paper, the response of a two pitches long and 2.5" internal diameter unbonded flexible pipe was numerically (ABAQUS-based FE model) and analytically analyzed when submitted to pure tension. The main goals of this work were to validate the numerical model both against experimental and previously published data; to study the influence of the contact parameters on the mechanical behavior of the pipe; and to determine its potential on further studies.

The analytical model showed more conservative results than numerical and experimental data. Numerical models, when subjected to pure tension, were noticed highly dependent on the normal contact stiffness and very little related to the variation of friction coefficient. As matter of fact, normal contact stiffness, if not well chosen, can generate a model with no physical correspondence. The best choice of parameters was 1000 N/mm³, for normal contact stiffness, and 0.10, for friction coefficient.

Finally, in addition to the good correlation between numerical and experimental results for global displacement and tendon's response, it is extremely important to highlight the significant potentiality of this model on the representation of more complicated behavior of tensile armor wire, such as stability problems.

## ACKNOWLEDGEMENTS

The first author would like to thank the *Conselho Nacional de Desenvolvimento Científíco e Tecnológico* (CNPQ) for the financial support, which contributed greatly to the development of the work.

## REFERENCES

Batista, R., Bogarin, J. and Ebecken, N., 1989. *Local mechanical behavior of multilayered flexible risers*. Proceedings of International Symposium on Offshore Engineering, COPPE/UFRJ, Rio de Janeiro.

Bathui, A., Bahai, H. and Alfano, G., 2008(a). *A finite element analysis for unbonded flexible risers under axial tension*. Proceeedings of the ASME 27th OMAE, 57627, Estoril.

Bathui, A., Bahai, H. and Alfano, G., 2008(b). *A finite element analysis for unbonded flexible risers under axial torsion*. In: Journal of offshore Mechanics and Arctic Engineering, 130.

Custódio, A. and Vaz, M., 2002. *A nonlinear formulation for the axisymmetric response of umbilical cables and flexible pipes*. Journal of Applied Ocean Research, 24, pp. 21-29.

Simulia (2013) - Abaqus 6.13 Online Documentation. [Online]. http://www.sharcnet.ca/Software/Abaqus610/Documentation/docs/v6.13

Feret, J., Bournazel C., Rigaud J., 1986. *Calculation of stress and slip in structural layers of unbonded flexible pipes*. In: Proc. of OMAE'86. New Orleans, USA: ASME.

Knapp, R., 1979. *Derivation of a new stiffness matrix for helically armored cables considering tension and torsion*. In: Journal of Numerical Methods, 14, pp. 515-529.

Merino, H., Sousa, J., Magluta, C., Roitman, N., 2009. *On the Coupled Extensional-Torsional Response of Flexible Pipes*. Proceedings of the ASME 28th OMAE, 79468, Honolulu.

Merino, H., Sousa, J., Magluta, C., Roitman, N., 2010. *Numerical and Experimental Response of a Flexible Pipe under Torsion*. Proceedings of the ASME 29th OMAE, 20902, Shangai.

NOV, 2015. *Webpage* obtained at: http://fps.nov.com/subsea/flexibles/dynamic-flexible-risers

Ramos, R., Martins, C., Pesce, C. and Roveri, F., 2008. *A Case Study on the Axial-Torsional Behavior of Flexible Risers*. Proceedings of the ASME 27thOMAE, 57514, Estoril.

Ramos, R. and Pesce, C., 2004. *A Consistent Analytical Model to Predict the Structural Behavior of Flexible Risers Subjected to Combined Loads*. In: Journal of Offshore and Mechanic Arctic Engineering, 126, pp.141-146.

Saevik, S., 1993. *A finite element model for predicting stresses and slips in flexible pipe armoring tendons at bending gradients.* Computer & Structures, 46:62.

Saevik, S.,2011. *Theoretical and Experimental Studies of Stresses in Flexible Pipes*. Computers & Structures, 89, pp.2273-2291.

Sousa, J., 2005. *Local Analysis of Flexible Risers Using the Finite Element Method*. DSc. Thesis, COPPE, Federal University of Rio de Janeiro, Rio de Janeiro, Brazil.

Witz, J., 1996. *A Case Study in the Cross-Section Analysis of Flexible Risers*. In: Journal of Marine Structures, 9: 885-904.

Witz, J. and Tan, Z., 1991. *On the axial-torsional behavior of flexible pipes umbilicals and marine cables*. Proceeding of Flexible Pipe Technology Seminar.